Journal of Molecular Graphics and Modelling 27 (2009) 665–675

Contents lists available at ScienceDirect

Journal of Molecular Graphics and Modelling

journal homepage: www.elsevier.com/locate/JMGM

Comparative modeling of thioredoxin glutathione reductase from *Schistosoma mansoni*: A multifunctional target for antischistosomal therapy

Monika Sharma [a], Smriti Khanna [a], Gopalakrishnan Bulusu [b,*], Abhijit Mitra [a,**]

[a] *Center for Computational Natural Sciences and Bioinformatics (CCNSB), International Institute of Information Technology (IIIT-H), Gachibowli, Hyderabad 500032, India*
[b] *Life Sciences R&D, TCS Innovation Lab Hyderabad, Tata Consultancy Services Limited, Madhapur, Hyderabad 500081, India*

ARTICLE INFO

Article history:
Received 18 June 2008
Received in revised form 7 October 2008
Accepted 27 October 2008
Available online 6 November 2008

Keywords:
Schistosoma mansoni
Thioredoxin glutathione reductase
Glutathione disulfide
Homology modeling
Docking

ABSTRACT

Schistosoma mansoni, a trematode parasite, which causes schistosomiasis and affects more than 200 million people worldwide, lives in an aerobic environment and therefore needs an effective redox mechanism for surviving reactive oxygen species from its host. Although, the host has two different redox systems: glutaredoxin and thioredoxin, the parasite has only one unique multifunctional enzyme, thioredoxin glutathione reductase (TGR) involving a fusion of two proteins, glutaredoxin (Grx) and thioredoxin reductase (TR), for performing all the redox activities. This dependence of *S. mansoni* on a single protein, TGR, for its protection from oxidative stress, makes it a promising drug target. Here, we describe a suitably validated, homology model for *S. mansoni* TGR (SmTGR), developed using both TR and Grx templates, functionally complete in the dimeric form with cofactors NADP(H) and FAD. Comparative analysis of substrate and inhibitor binding pockets of our model with crystal structures of parent TR as well as with that of glutathione reductase (GR), which is an essential component of the Grx system, appears to provide greater insight into the functioning of TGR. This also augments recent observations reported on the basis of X-ray structure data on SmTGR monomer lacking the C-terminal selenocysteine tail.

1. Introduction

Schistosomiasis, or bilharzia, is a tropical disease that is endemic in 74 developing countries and infects more than 200 million people (mostly children under 14) in rural and sub-urban areas according to the World Health Organization (WHO) [1]. The causative organisms of schistosomiasis are trematode parasites that belong to the genus *Schistosoma*. Species like *Schistosoma mansoni*, *S. japonicum*, *S. mekongi* cause intestinal schistosomiasis, whereas *S. haematobium* causes urinary schistosomiasis. Schistosomiasis is second only to malaria in public health importance and hence, demands urgent attention [1]. Currently available drugs include praziquantel (effective in the treatment of all forms of disease), oxamniquine (for intestinal type caused by *S. mansoni*) and metrifonate (for urinary schistosomiasis) [1]. Since the chemotherapy is limited, temporary and prone to resistance, development of vaccines is a challenging alternative [2]. Sequencing of the parasite genomes, manipulating gene expression and understanding gene function, promise faster identification of targets for diagnostics, drugs and vaccines [3].

S. mansoni lives in an aerobic environment and therefore needs an effective redox mechanism for its survival in the host. In eukaryotes, there are two major thiol-dependent redox pathways: glutaredoxin (Grx) and thioredoxin (Trx) [4,5]. The Grx system consists of (i) glutathione reductase (GR), a member of the pyridine nucleotide disulfide oxidoreductase family, which is a homodimer of 55 kDa subunits having a disulfide CXXXXC motif in the active site [6,7], (ii) glutathione or GSH, a γ-Glu-Cys-Gly tripeptide, (iii) Grx, an 11 kDa thiol/disulfide oxidoreductase with CXXC redox motif and (iv) GSH peroxidase (GPx). GR catalyzes the reduction of diglutathione or glutathione disulfide (GSSG), bound at the GR dimer interface, to two reduced GSH molecules *via* a series of electron transport processes shown in Fig. 1. The Trx system is

* Corresponding author. Tel.: +91 40 66673591; fax: +91 40 66672222.
** Corresponding author. Tel.: +91 40 23001967x171; fax +91 40 23001413.
E-mail addresses: gopal@atc.tcs.com (G. Bulusu), abi_chem@iiit.ac.in (A. Mitra).

Abbreviations: WHO, World Health Organization; Grx, Glutaredoxin; Trx, Thioredoxin; GR, Glutathione Reductase; GSH, Glutathione; GPx, Glutathione Peroxidase; GSSG, Glutathione disulfide; TR, Thioredoxin Reductase; TPx, Thioredoxin Peroxidase; SeC, Selenocysteine motif; TGR, Thioredoxin Glutathione Reductase; SmTGR, *Schistosoma mansoni* TGR; FAD, Flavin Adenine Dinucleotide; NADP(H), Nicotinamide Adenine Dinucleotide Phosphate; RMS, Root Mean Square deviation; SSM, Secondary Structure Method of superposition; SMD, Steered Molecular Dynamics.

1093-3263/$ – see front matter © 2008 Elsevier Inc. All rights reserved.
doi:10.1016/j.jmgm.2008.10.009

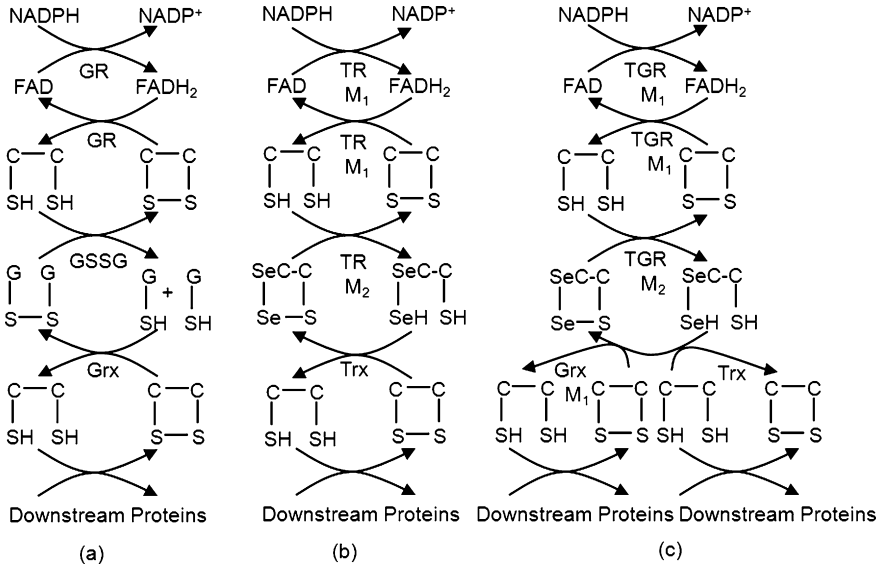

Fig. 1. Electron transport process in (a) GR: Grx pathway—the reaction proceeds with the concomitant oxidation of NADP(H) *via* FAD and CXXXXC disulfide motif. Reduced GR goes on to reduce GSSG resulting in two GSH molecules and in the process it gets oxidized, regenerating the disulfide bridge. GSH further reduces other proteins like GPx and Grx. Reduced Grx performs various Grx-dependent reactions like reduction of various substrates and substrate-related reductases like ribonucleotide reductase (b) TR: Trx pathway—electron transfer mechanism is the same in TRs as GRs except for additional involvement of the SeC motif. The amino terminal redox active disulfide (CXXXXC) of one subunit is reduced by NADP(H) *via* the FAD of the same monomer (M1), thereafter interacting with the C-terminal SeC of the other monomer (M2) which lies close to it. TR reduced at the SeC motif, reduces Trx and itself gets back to the oxidized sate. Reduced Trx performs various Trx-dependent reactions such as providing reducing equivalents to other redox enzymes like TPx and ribonucleotide reductase. (c) TGR: the redox disulfide in TR domain of one monomer (M1) of TGR is reduced by the NADP(H) *via* FAD which reduces the SeC motif of the second monomer (M2). The reduced SeC motif at the C-terminal in TGR then serves the role of a protein-linked GSSG and shuttles electrons to either the Grx domain of M1 or Trx. Thus TGR can coordinate both Grx and Trx-dependent reactions.

composed of (i) thioredoxin reductase (TR), homodimer of 56 kDa subunits, analogous to GR, (ii) Trx, a 12 kDa thiol/disulfide oxidoreductase with redox active CXXC motif and (iii) Trx peroxidase (TPx). Three mammalian TR isozymes TR1 (cytosolic), TR2/TGR and TR3 (mitochondrial) are known. Unlike GR, TRs contain a C-terminal extension that terminates with a conserved tetrapeptide sequence Gly-Cys-SeC-Gly, known as SeC motif (Fig. 2), which is an important component of the electron transfer process [8,9] (Fig. 1).

Unlike TR1 and TR3, TGR or thioredoxin glutathione reductase [10,11], is a fusion of TR with Grx at the N-terminus (Fig. 2). Since Grx is a part of a related albeit different redox system, TGR exhibits specificity for both redox systems (Fig. 1) and this provides TGR with wider substrate specificity [12–14]. SmTGR thus appears to be a single major redox enzyme in *S. mansoni*, completely replacing TR and GR which are functional in its host [15], and is therefore an important drug target for *S. mansoni* [16]. There are a few biochemical studies throwing light on the functional aspects of this protein, reported so far [15,16]. However, a thorough understanding of the functional mechanism, elucidated through extensive biochemical studies and validated on the basis of three-dimensional (3D) structure of the fully functional target, is essential for exploiting the potential of TGR as a therapeutic target. The recently solved crystal structure of SmTGR is that of a monomer with only one cofactor, FAD and without the other cofactor, NADP(H) as well as the SeC tail [17]. Though the structure has shed greater light on the mechanistic details, several issues are yet unclear:

(a) In the species wherein separate Grx and Trx systems operate, there are three essential oxidoreductase activities: (1) TR—Trx (Trx-dependent reactions), (2) GR—GSSG/GSH (GSH-dependent

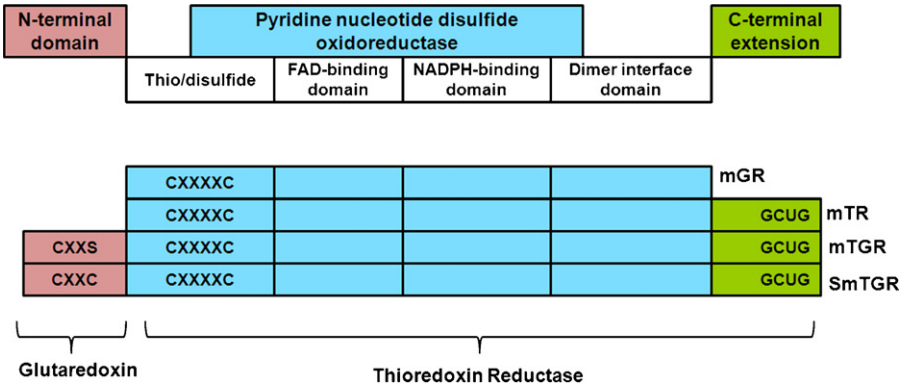

Fig. 2. Comparative domain organization of mammalian GR, TR, TGR and SmTGR. GR contains FAD and NADP(H) binding sites, active site redox center and dimer interface domains. TR has an additional C-terminal extension of GCUG or the SeC motif (U is selenocysteine residue). TGR is a fusion of TR with glutaredoxin at the N-terminus. mTGR and SmTGR differ in the CXXC disulfide of Grx domain wherein one of the cysteines is replaced by a Serine in mTGR.

reactions), (3) GSSG/GSH—Grx (Grx-dependent reactions). In SmTGR, however, where TR and Grx are fused together, the question arises as to how it performs GR activities!

(b) The C-terminal SeC tail is essential for various redox processes in TR and SmTGR, the absence of which in the crystal structure limits our understanding of the mechanistic details. In GR, where the SeC tail does not exist, reduction of GSSG to GSH takes place at the FAD/disulfide active site which is required for Grx activation. In TR dimer, the role of the GSSG/GSH couple is taken over by the C-terminal SeC motif of the partner monomer for Trx activation. In SmTGR, however, the role of GSSG/GSH couple and/or the SeC tail for Grx and Trx activation requires clarity. It has been proposed that the SeC domain possibly acts as a shuttle, alternating electron transport from the FAD/disulfide active site to the Grx or Trx domain [12]. The active site disulfide of Grx, in the SmTGR dimer, appears to be far away from the C-terminal SeC motif for electron transfer from the SeC motif to take place. Biochemical experiments show that though TR does not show GR activity, TGR does [17]. Experiments involving truncated TR and SmTGR, where the SeC tails were removed, also showed total absence of GR activity with TR but definite, albeit reduced, GR activity with SmTGR [17]. Thus, the SeC motif does not seem to be essential for GR activity of SmTGR.

(c) The Grx domain of SmTGR can be functional in the presence of GSH generated externally [17], and may not require SeC tail for Grx activation. However, the possibility of parallel pathways, one implicating the SeC domain and the other implying-independent GR activity of TGR cannot be ruled out as mechanisms for Grx activation. The latter pathway is possible if TGR has a GSSG binding domain which is similar to that of GR, or the Grx domain, activated through the participation of the SeC motif in the TGR dimer, performs the GSSG to GSH reduction when GSSG concentration exceeds a certain threshold.

(d) Another issue that needs to be addressed is the interdomain movements, both within a monomer as well as between two monomers in the dimer, in terms of transitions between oxidized and reduced forms of TGR. An understanding of this is important from the point of view of mechanistic clarity. It may be pointed out, that large conformational changes involving the FAD and NADP(H) domains have been implicated in *E. coli* TR [18]. Similarly, comparative study of different X-ray structures of TRs reveal two distinct relative orientations of the FAD and NADP(H) molecules in terms of *pi*-stacking of the flavin ring of FAD with the nicotinamide ring of NADP(H) [19,20]. The relative movement of the SeC domain of monomer 2 with respect to the Grx domain of monomer 1, in the TGR dimer is another issue demanding clarity. The absence of NADP(H) in the crystal structure makes such analysis difficult. Therefore, a proper understanding of the functional dynamics related to the substrate (Trx, Grx and GSSG) binding and redox mechanism needs a validated model of the fully functional dimer of SmTGR. This is especially true since the alternative mechanistic proposals, as discussed above, differ on the relative importance assigned to 'within monomer' and 'across dimer' electron transfer processes.

Herein we present our efforts at analyzing some of the above mentioned aspects on the basis of homology models, containing both the cofactors FAD and NADP(H), developed for the functional dimer of SmTGR, validated by molecular docking studies with both GSSG as well as with known inhibitors of homologous proteins like GR.

2. Methods and computational details

Two models, putatively corresponding to 'reduced' and 'oxidized' forms of SmTGR, were generated. The two cofactors NADP(H) and FAD, oriented respectively in two different states, were added to an initial homology model of the monomer of SmTGR before generating the final dimer structures. Apart from standard refinement and evaluation protocols involving energy minimization, molecular dynamics (MD) simulations, torsion angle checks and checks for short contacts, detailed validation of the final models was carried out for their compatibility with available biochemical data. Our approach and its rationale, along with relevant computational details are summarized below.

2.1. Homology modeling of the monomer

The sequence of SmTGR, composed of 598 amino acids (from NCBI, accession code AAK85233) was submitted for BLAST search against protein data bank to retrieve homologs with available 3D structures. As TGR is a fusion of two different proteins, the first 110 residues of the N-terminus showed close similarity with Grx and the last 488 residues showed similarity with other proteins such as TR and GR. Sequences showing good similarity (*E*-value $\leq$ 1E−04) with the reference *S. mansoni* sequence were used for generation of the initial homology model. Three best templates were chosen for N-terminal region and four templates for the rest of the protein (Table 1, Figure S1).

Homology modeling was carried out using MODELLER 9v1 [27]. All the above template structures were employed for generating the monomer model of SmTGR. Both Grx and TR regions of SmTGR have active site disulfide bridges C28–C31 and C154–C159 which were incorporated in the model by generating disulfide patches during homology modeling.

2.2. Generation of the dimer

The functional unit of the protein is reported to be dimeric [11,13]. Although TR and GR adopt similar global fold, SmTGR

Table 1
Protein templates used for homology modeling of SmTGR with their PDB codes, type of protein, sequence identity (SI), number of residues and the *E*-value with respect to the whole sequence.

S. no.	PDB	Protein type	SI (%)	Residues	*E*-Value	Ref.
N-terminus						
1	1Z7P	Glutaredoxin C1 from *Populus tremula* X Tremuloides	36	107	5E−12	[21]
2	1B4Q	Human Thioltransferase	25	94	1E−04	[22]
3	1KTE	Thioltransferase from *Sus scrofa*	25	100	2E−04	[23]
C-terminus						
1	2CFY	Human Thioredoxin Reductase 1	60	484	2E−154	[24]
2	1H6V	Rat Thioredoxin Reductase	60	490	1E−152	[25]
3	1ZDL	Mouse Thioredoxin Reductase Type 2	54	484	3E−141	[19]
4	2NVK	Thioredoxin Reductase from *Drosophila melanogaster*	51	481	7E−127	[26]

showed greater homology to TR (50–60%) than GR (36%). The initial model of the monomer, generated as described above, was also found to share greater structural similarities (Figure S2) with TR monomers. Therefore, a template comprising of the dimeric structure of TR (2J3N) [20] was used to prepare the dimeric model of SmTGR by superposing minimized monomer structures (as described under 'refinement of models') on the template using SYBYL7.1 from Tripos Inc. [28].

2.3. Addition of cofactors to the dimeric model

Positioning of cofactors FAD and NADP(H) needed thoughtful consideration. It is reasonable to hypothesize that, corresponding to the electron transfer sequence during its redox cycle, the 3D structure of SmTGR goes through three distinct conformational states: (a) entry of NADPH into its designated pocket, (b) transfer of reducing equivalents from NADPH to FAD for onward progression of the redox cascade and (c) exit of NADP.

The fact that the SmTGR sample used for the crystal structure study [17] could not be co-crystallized with NADP(H), may be suggestive of the structure being in the conformational state "c" described above. More concrete validation for the existence of alternative conformational states came from our analysis of published crystal structures of TR [19,20], where two different orientations of NADP(H) were observed with respect to FAD. In the mouse TR structure (1ZDL) [19], nicotinamide ring of NADP(H) was found to be in a *pi*-stacked orientation (conformation I) with flavin ring of FAD [19]. Analysis of the human TR structure (2J3N) [20], however, revealed that the two rings are far apart from each other and constitute a non-*pi*-stacked structure (conformation II). Clearly the two conformations differ greatly, both in terms of conformations as well as in terms of their relative disposition (Table T1).

The 'conformational state' hypothesis can be extended not only to correlate the conformations I and II with reduced and oxidized conformations of TR, respectively, but also to suggest similar conformational transitions to be occurring in TGR. Therefore, two models were constructed, one for the reduced conformation and the other for the non-reduced conformation, by incorporating the cofactors into the respective pockets in two different orientations (Fig. 3). Although the two holo models were generated by introducing the cofactors, in different conformations in the same apo model, the amino acid environment of the cofactors in the two models assumed distinct characteristics after the refinement steps described in the next section [29].

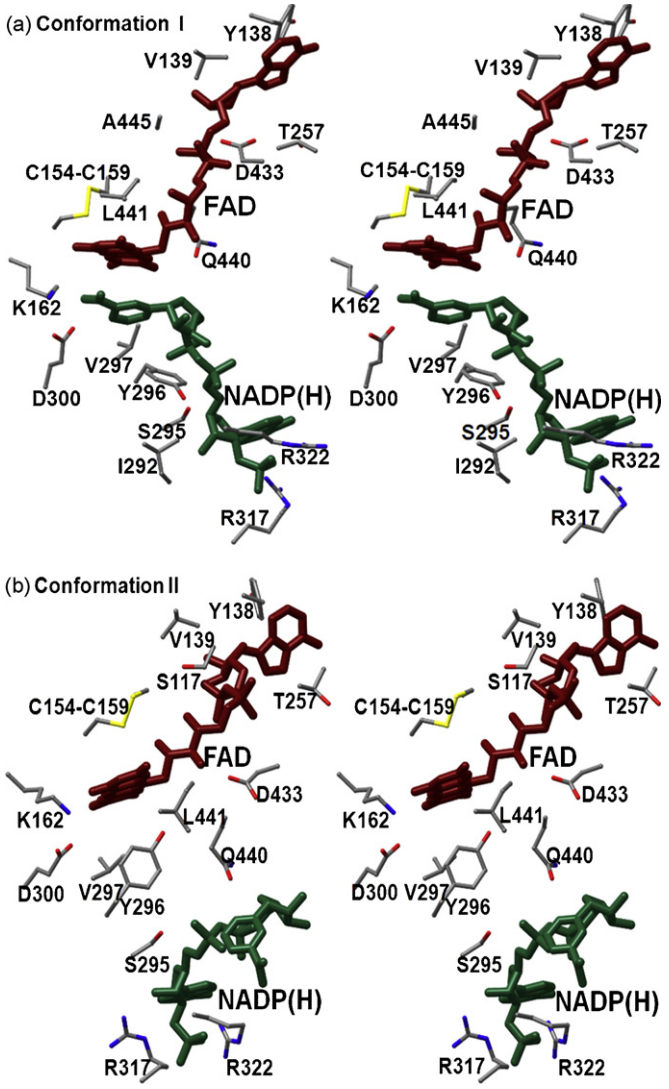

Fig. 3. Stereo view of the two conformations in which cofactors FAD and NADP(H) are found. (a) Conformation I is the reducing, *pi*-stacked conformation in which the flavin ring of FAD (in maroon) and nicotinamide ring of NADP(H) (in dark green) are stacked and (b) conformation II is the non-reducing, non-*pi*-stacked conformation in which these rings are apart. Residues interacting with cofactors within 4 Å distance are shown. Residues Tyr296, Gln440 and Leu441 occupy the space created when the nicotinamide ring of NADP(H) moves out of *pi*-stacked conformation.

2.4. Refinement and evaluation of the models

NAMD2.6 [30] with CHARMM22 force fields were used for optimization of both monomer and dimer models. The dimer was further minimized after incorporation of FAD and NADP(H). The proteins were solvated in a 7 Å layer of TIP3P [31] water and neutralized. Periodic boundary conditions were employed to eliminate surface effects. For full electrostatic computations, particle mesh Ewald (PME) [32] was used with tolerance of 1E−05 and grid-spacing of 1.0 Å. Langevin dynamics was used to control temperature and pressure parameters (NPT). Energy minimization was done on the whole system till the gradient tolerance was less than 0.5. Monomer was minimized for 50,000 cycles and dimer was minimized for 100,000 cycles. During minimization, the backbone was kept fixed initially and then the whole structure was minimized with restrained Cα atoms. During dynamic simulation after minimization, monomeric system was heated from 0 to 300 K in 55 ps. For dimeric system, simulated annealing was done wherein the system was heated from 0 to 350 K, with an increment of 10 K/ps and cooled to 298 K at the rate of 4 K/ps. Finally, both the monomeric and the dimeric systems were equilibrated for 100 ps. Simulations for the monomer were done at time step of 0.1 fs and for the dimer at 0.2 fs. Analysis of the protein structures was carried out using built-in programs of VMD 1.8.6 [33].

The models, after optimization, were evaluated with PROCHECK suite of programs [34]. The *phi–psi* plot for the final dimer model is shown in Fig. 4 and detailed results are listed in Table 2. Ramachandran plot of the model showed a normal distribution of points with *phi* angles mostly restricted to negative values. The values for all nonglycyl, nonprolyl residues occurred in the most favored regions (89.6%), additional allowed regions (8.5%), and generously allowed regions (1.1%). Only five residues per monomer (1.1%) were present in the disallowed regions. Fig. 4 shows the overall structure to be reasonably good.

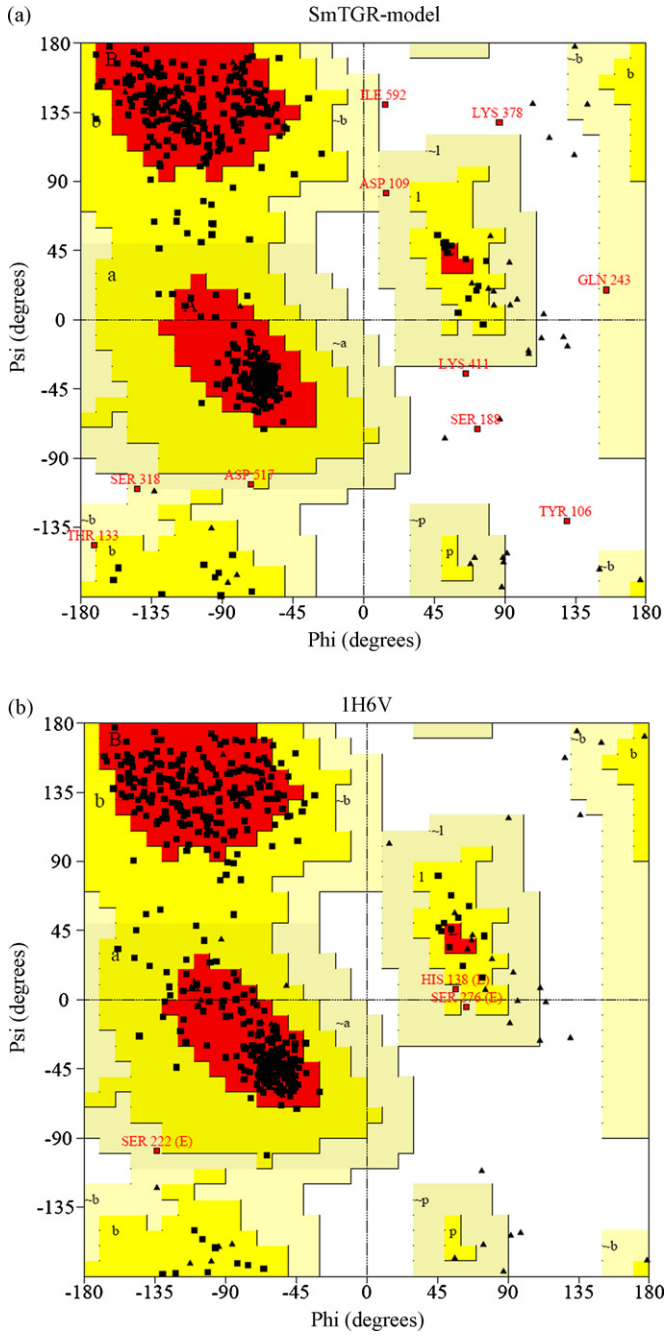

Fig. 4. Comparison of the Ramachandran plot of monomeric SmTGR model with crystal structure of one of the template TRs with PDB code 1H6V. The comparative numerical values are given in Table 2.

Table 2
Results of protein structure evaluation of SmTGR model by PROCHECK in comparison to one of the template TRs.

Residues	SmTGR	1H6V
Residues in most favored regions	463 (89.6%)	354 (84.7%)
Residues in additionally allowed regions	44 (8.5%)	61 (14.6%)
Residues in generously allowed regions	5 (1.1%)	3 (0.7%)
Residues in disallowed regions	5 (1.1%)	0 (0.0%)
End residues (excl. Pro and Gly)	1	1
Number of glycine residues (shown as triangles)	57	52
Number of proline residues	23	19
Total number of residues	598	490
Overall PROCHECK residues[a]	−0.21	−0.15

[a] Recommended values of PROCHECK scores is >−0.5.

2.5. Model compatibility with biochemical data

Molecular docking and steered molecular dynamics studies were carried out with the models generated as above.

2.5.1. Docking with GSSG

TGR has greater similarity with TRs than GRs, both in terms of sequence as well as structure. However, biochemical experiments showed that, while TGR has limited GR activity, TR has none. The crucial factor, which might be influencing this behavior, is the variation in the binding pocket of GSSG, the substrate for GR. Therefore, GSSG has been docked in GR, TGR as well as TR to evaluate their relative binding. The crystal structure of GR complexed with GSSG (1GRA) [35] was used for docking. Since it exists as a monomer, it was 'dimerized' to analyze the contribution of the second monomer. Similarly, GSSG extracted from 1GRA was docked in TR (2J3N) [20], SmTGR model and SmTGR crystal structure (2V6O) [17]. TR and SmTGR model have SeC tails that obstruct the path of GSSG in its binding pocket. The SeC tails were therefore, displaced by modifying their backbone torsions. The active site was defined as a sphere of 8 Å radius around the substrate. The protein was assigned with Kollman charges and the cofactors and the substrate with Gasteiger-Huckel charges.

2.5.2. Docking with inhibitors of homologs

The correctness of the fold, and its significance, near the active site and the dimer interface of TGR needed to be tested. Three crystal structures of GR-inhibitor complexes, which are close homologs of TGR, were found in the protein databank. The ligands extracted from these complexes were used for molecular docking studies with the homology model of SmTGR using Flexidock [36] module within the SYBYL package (Table 3).

SmTGR dimer model was employed to generate docking input files. The GR protein with the corresponding inhibitor was superposed with the SmTGR model. The inhibitor was extracted from GR-inhibitor complex and merged with SmTGR in the corresponding binding pocket. Active site was defined as an 8 Å sphere of radius around the ligand. Kollman and Gasteiger-Huckel charges were assigned to the protein and the ligand/cofactor atoms, respectively. Important donor and acceptor sites were defined on the ligand as well as on the receptor. Docking runs for each of the ligands generated 20 different docked poses.

GROMACS 3.3.1 [40] was used for minimization of docked structures employing GROMOS 96 force field. Parameters for cofactors and ligands were obtained from Dundee-PRODRG2 server [41]. Structures were solvated in SPC model water box leaving at least 8 Å between solute atoms and boundaries of box. PME was used for electrostatic interactions. Minimization was done, first by steepest descents till energy tolerance limit of 1000 kJ/mol followed by conjugate gradient methods till 100 kJ/mol as tolerance limit.

2.5.3. Hinge movement of Grx domain

The viability of electron transfer in terms of distance from the SeC motif (monomer 2) to Grx domain (monomer 1) has been

Table 3
Glutathione reductase (GR)-inhibitor complexes used for docking and the nature of the protein-inhibitor bond in them.

S. no.	PDB	Ligand	Bond-type	Ref.
1	1XAN	Xanthene-der[a]	Non-covalent	[37]
2	1BWC	Adjoene-der	Covalent	[38]
3	2GH5	Menadione-der	Covalent	[39]

[a] der: derivative.

questioned [17]. Steered molecular dynamics experiments were carried out to observe the hinge movements of Grx domain. Since the focus is only on the movement of Grx domain, hence only this domain was allowed to move and the rest of the protein was held fixed. Simulation was carried out using NAMD2.6. Forces were applied with force constant, $K = 350$ pN/Å and velocity, $\upsilon = 0.002$ Å/ps at 300 K.

3. Results and discussion

Although apparently the only significant structural difference between GR and TR is the C-terminal extension containing the SeC motif (Fig. 2), it is known that functionally TR differs from GR in the sense that it cannot reduce GSSG. One of the central questions, therefore is, how does TGR replace all three proteins (TR, GR and Grx) and perform activities related to all of them in *S. mansoni*.

3.1. Analysis of the SmTGR dimer models

The large TR domain forms the head of the protein which connects to its tail formed by the Grx domain *via* a small linker loop. The dimer generated from the TR templates brings the two TR regions together and the Grx domains are placed diagonally apart (Fig. 5). Overall, the dimer can be classified structurally into different domains: (a) N-terminal Grx domain with a characteristic GSH-binding motif (CXXC), (b) NADP(H) and FAD-binding domains, (c) thiol/disulfide redox active center (CXXXXC), (d) dimer interface domain and (e) C-terminal extension terminating with conserved Gly-Cys-SeC-Gly (Figure S4). The dimer has three active disulfide redox centers: Cys28–Cys31 in Grx domain, Cys154–Cys159 near the FAD and NADP(H) binding site in TR domain and Cys596–SeC597 at the C-terminus. As required, the mobile C-terminal SeC motif of the second monomer is found in close proximity and accessible to the disulfide in TR region for effective electron transfer from cofactors to substrates or downstream proteins. However Grx domain, which in principle should be proximal to this SeC motif for the next electron transfer, lies farther at a distance of 37 Å.

3.2. Pi-stacked vs. non-pi-stacked models

The two models of SmTGR, differing in the orientation of cofactors were compared. On superposition, the RMS deviation was calculated to be 2.34 Å (Figure S5). The overall structure does not exhibit major differences except slight side chain movements of some residues in FAD and NADP(H) binding pockets (Fig. 3). As cofactors transit from *pi*-stacked to non-*pi*-stacked conformation, a major reorientation of the side chains of Tyr296, Gln440 and Leu441 was observed. In conformation II, Tyr296 becomes perpendicular to the FAD flavin ring when NADP(H) moves out of *pi*-stacked orientation, and forms CH-π interactions with the FAD ring. The two positions are analogous to Tyr228 in the mouse TR (1ZDL) [19] which is in reducing conformation and Tyr200 in the human TR (2J3N) [20] which is in non-reducing conformation. A similar movement of Tyr197 is reported for GR when nicotinamide ring of NADP(H) has to adjust near FAD (1GRA) [35]. Gln440 which corresponds to Glu366 in 1ZDL and Glu341 in 2J3N also reorients itself along with Leu441, to fill in the gap introduced when NADP(H) ring moves out of stacked conformation. Other important interactions observed with NADP(H) in 1ZDL are the salt bridges of 2′-phosphate group with two arginine residues (Arg249 and Arg254) and H-bonds of one of the bridging phosphate groups with Ser227, Val229. In 2J3N, though corresponding salt bridges with Arg221 and Arg226 are observed, the H-bonds with the corresponding Ser199 and Val201 residues are however affected by the movement of NADP(H) ring. In our models too, the H-bonds with the corresponding Ser295 and Val297, and the salt bridges with the corresponding Arg317 and Arg322 are affected during this transition.

3.3. SmTGR homology model comparison with crystal structure

While this manuscript was in preparation, the crystal structure of SmTGR appeared (2V6O) [17], and we have compared our homology model with it. The crystal structure is in the monomeric form and did not include NADP(H). Apparently, NADP(H) could not be co-crystallized with the protein. The characteristic SeC motif in the C-terminus is also missing in the crystal structure. Superposition of the crystal structure with our models using secondary structure method (SSM) of superposition [42,43] brings out their close similarity (Fig. 6). SmTGR model with conformation II (non-reducing form) shows smaller RMSD of 1.62 Å as compared to conformation I with RMSD of 3.78 Å in the TR region. In the non-reducing model, FAD fits in the same pocket and has similar orientation as in the crystal structure. NADP(H), absent in the crystal structure, fits well in its empty binding pocket. Tyr296 in 2V6O lies perpendicular to the FAD ring as observed in conformation II of our model. This implies that the TR domain of the crystal structure is similar to the non-reducing conformation of our model (RMSD: 1.62 Å).

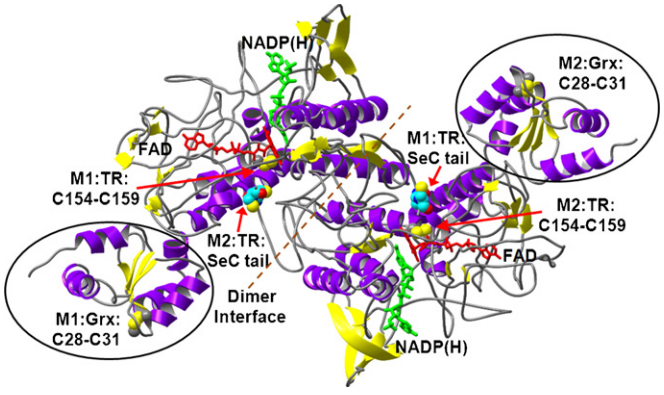

Fig. 5. The dimer model for SmTGR is shown with various domains in two monomers (M1 and M2). NADP(H) is shown in dark green, FAD in maroon, and the disulfides are shown in yellow spacefill.

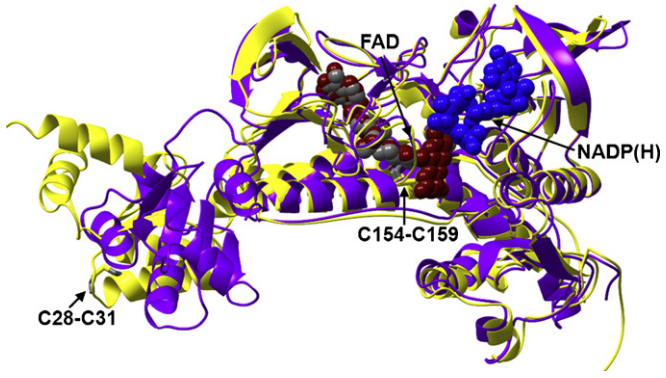

Fig. 6. Superposition of SmTGR crystal structure (in purple) with homology model (in yellow) in conformation II. RMSD between the TR domains of the two structures is 1.62 Å. FAD in the crystal structure is shown in maroon, while in the model it is shown in grey. NADP(H) in the model (not present in the crystal structure), is shown in blue.

3.4. Grx domain and hinge movement

The Grx region of our model shows some variance with the crystal structure. The Grx domain in 2V6O [17] seems to be folded inwards towards the TR domain and should be closer to the SeC tail of the second monomer had it been there. This position may be inferred as the 'closed' form. However, in our model, the Grx domain is positioned away from the TR domain and can be referred to as the 'open' form. This difference can be attributed to either the inherent process of homology modeling or the movement of Grx domain due to the presence of a flexible linker loop connecting Grx and TR domains. To simulate the domain movement of Grx, hinge movement analysis through steered molecular dynamics (SMD) (Fig. 7) was carried out. SMD studies showed that the Grx domain of one monomer can actually move towards the C-terminal tail of second monomer. Simultaneously, the SeC tail may also move towards the Grx domain. Hence, relative movement of the two domains can bring the two redox centers close enough for electron transfer.

From the comparative study of the model with 2V6O [17], we speculate a slight transition of one redox conformation to another during different steps in the electron transfer process. When NADPH enters its site of action near FAD, SmTGR is found in reducing conformation I. After it does its job, NADP flips, with the corresponding rearrangement of adjoining residues (described in the previous section) and morphs into non-reducing conformation II. $FADH_2$ then transfers reducing equivalents to the active site disulfide Cys154–Cys159. The reduced disulfide goes on to reduce the proximal SeC disulfide of the second monomer which lies close it. The reduced C-terminal SeC tail being flexible could transfer electrons to Cys28–Cys31 disulfide in Grx domain, if it is in the "closed" position, or to the substrate. After the electron transfer process, Grx can revert to "open" form. This hypothesis requires elaborate biochemical studies of the mechanism of electron transfer. However, it should be noted that TR and Grx domains can work either coupled or independently since Grx can accept electrons from fused TR domain or from free GSH [17]; and Grx flexibility can allow Trx to bind in its place. Likewise, TR domain can donate electrons to either fused Grx or Trx, resulting in competition between them.

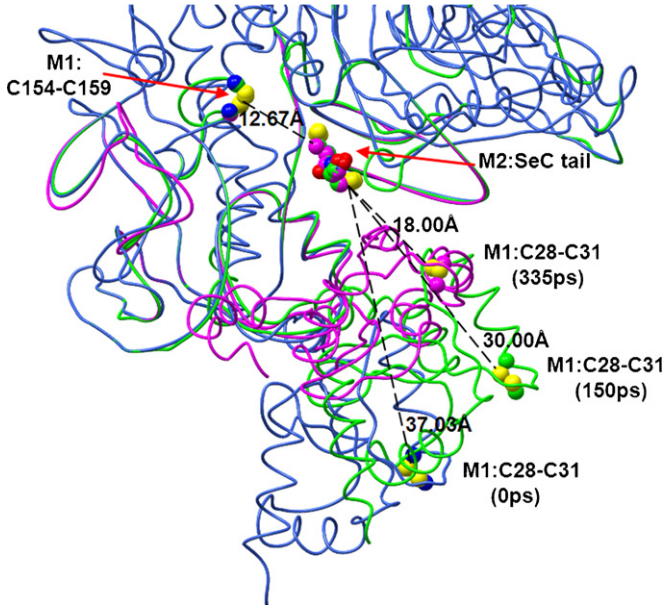

Fig. 7. Snapshots of hinge movements of Grx domains *vis-a-vis* TR domain. Distances are shown between the respective redox centers. Snapshot at 0 ps is shown in blue, at 150 ps in dark green, and at 335 ps in maroon. The distance is reduced from 37.03 to 18.00 Å.

3.5. Molecular docking studies

In order to validate the homology model, docking of substrates and inhibitors of the template proteins was carried out. GSSG reduction, which is the normal function of GR, shows ambiguous trends in TR and TGR in spite of their reasonably good homology with GR. Hence, comparative docking studies were performed in GR, TR, SmTGR model and in the crystal structure of SmTGR with GSSG to find their binding affinities. Some of the inhibitors of GR were also docked in the binding site of our SmTGR model.

3.5.1. GSSG docking

In GR (1GRA) [35], the four armed GSSG substrate is anchored close to FAD and the active site disulfide motif (Cys58–Cys63). Various H-bonding residues with the substrate are listed in Table 4. Of these, Tyr114 plays a major role by forming H-bonds with the –NH groups of the γ-glutamyl moieties in two of the arms of GSSG. Arg37 and Arg347 form salt bridges with the terminal $-COO^-$ groups of GSSG (Fig. 8). This pose of GSSG brings it close to the active site disulfide (Cys58–Cys63) where it is accessible for reduction.

In human TR (2J3N) [20], an analogous GSSG binding pocket near the FAD and disulfide motif (Cys59–Cys64) exists. H-bonding residues, analogous to GR are shown in Table 4. Tyr116, Arg351 and Lys29 in TR correspond to Tyr114, Arg347 and Arg37 of GR, respectively. Although, the GSSG binding site appears conserved, the major hindrance to GSSG binding is posed by the SeC motif of the second monomer that obstructs H-bonds with Tyr116. The obstruction by the SeC motif was deemed as an important factor for inactivity of TR towards GSSG binding [25]. However, TR without SeC tail was also able to reduce GSSG [44]. Additional factors related to contrasting electrostatic environment between TR and GR have been proposed for the same [44].

SmTGR model with GSSG in the corresponding binding pocket exhibits interactions with Tyr212, Lys124 and Arg450 side chains as in GR (Table 4). The SeC tail, considered important for the GR activity of TGR, as per earlier biochemical studies [15], is in close proximity to the GSSG binding pocket as in TR. It is interesting to note that though TR does not reduce GSSG, TGR which is a fusion of

Table 4
Comparison of residues which aid in anchoring GSSG in its binding pocket near FAD and active site disulfide, in GR, TR and SmTGR crystal structures.

S. no.	GR (1GRA)	TR (2J3N)	TGR (2V6O)
Monomer 1			
1	M406	L409	L508
2	H467	H472	H571
3	T469	V474	T573
4	S470	C475	–
5	E472	E477	E576
6	E473	–	T577
7	T476	T481	T580
8	–	W407	K506
Monomer 2			
9	S30	S22	S117
10	A34	–	–
11	R37	K29	K124
12	K67	–	K163
13	Y106	H108	–
14	Y114	Y116	Y212
15	N117	–	–
16	R347	R351	R450

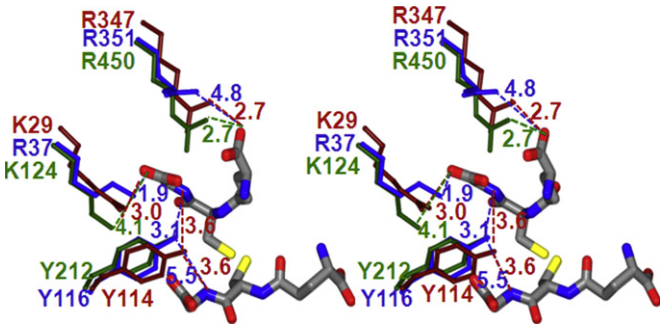

Fig. 8. Stereo view of important residues interacting with GSSG substrate in GR (shown in maroon), TR (shown in blue) and TGR (shown in dark green). Few interaction distances are also shown.

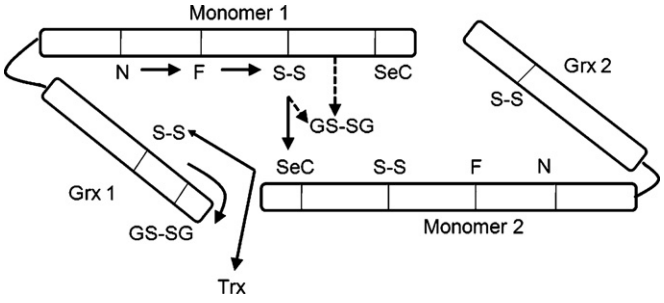

Fig. 9. Electron transfer process in SmTGR indicated by arrows from N (NADP(H) to F (FAD) to S–S (active site disulfide in TR domain) to C-terminal SeC motif of the second monomer and finally to either S–S (active site disulfide in Grx domain) or to Trx. Two pathways of electron transfer to GSSG have been proposed: GSSG located near the FAD binding site is reduced by the direct electron transfer from F while GSSG located in the Grx domain is reduced by reduced Grx domain.

TR and Grx, performs this activity [11]. But, how does TGR reduce GSSG?

Recently, two pathways for GSSG reduction in SmTGR have been proposed based on biochemical evidence that provide possible answers (Fig. 9) [17].

- The biochemical studies on SmTGR without the SeC motif exhibit, although low, but measurable GR activity indicating direct reduction of GSSG near the FAD site [17]. The crystal structure clearly shows the existence of a putative GSSG binding site in this region, which is filled with water molecules in the absence of GSSG. The GR activity shown by truncated SmTGR may be attributed to the fact that hindrance posed by the SeC tail is absent. However, this possibility can be overruled as truncated TRs are unable to exhibit GSSG reduction as mentioned before [44]. Another factor that strengthens this viewpoint is the electrostatic environment of the binding site. Electrostatic potential of this pocket has been found to be similar to GR which is in contrast to TR. These two factors indicate that the GSSG binding pocket in SmTGR may be the same as in GR [17].
- A second site for GSSG reduction has been proposed in the Grx domain [17] of SmTGR (Fig. 9). This requires internal electron transfer to the Grx domain as seen in *Taenia Cressiceps* [45]. The reduction process is concentration dependent. High concentrations of GSSG may result in GSSG binding to Grx domain and its subsequent reduction therein [45].

Alternatively, we suggest another indirect pathway which may also be operational in SmTGR. It is known that GSSG is a substrate of reduced Trx. [4]. Reduction of Trx corresponds to the TR activity of SmTGR. Reduced Trx may reduce GSSG in cells with increased GSSG level but inadequate GR activity [46].

Since the electrostatic environment in the GSSG binding pocket near the FAD site has been proposed to be a major factor contributing to the reduction of GSSG in GR, TR and SmTGR, the active site residues within a sphere of radius 15 Å around GSSG have been analyzed. All the positively charged (histidine, lysine and arginine) and negatively charged (aspartic acid and glutamic acid) residues were accounted for, to calculate the total formal charge residing in the active site. Indeed, as expected, GR has the highest total positive charge of 12 units while TR has the lowest of 7 units. TGR falls intermediate between the two with 9 units (Fig. 10). The electrostatic potential surface generated for the active site region depicts GR with the maximum positive charge (0.1219), TGR with intermediate (0.0602) and TR with the least (−0.0199) (Figure S6). This may as well explain the lower GR activity exhibited by the truncated SmTGR as compared to GR by Angelucci et al. [17].

To explore the differences in GSSG binding in GR, TR and SmTGR near the FAD site further, docking studies were performed with these proteins. The docking scores of GSSG show comprehensive trend in their binding affinity in all the three systems (Table 5). GR exhibits the best binding score followed by SmTGR crystal structure and homology model and finally by TR. Thus, the docking studies also support favorable GSSG binding in SmTGR as compared to TR.

3.5.2. Inhibitor docking

Inhibitor docking studies were carried out to compare the protein folds of SmTGR homology model with the homologous

TGR	K124	E125	K128	D137	-	K162	K163	H166	V201	H204	S207	K213
TR	K29	E30	Q33	D42	-	K67	K68	H71	V105	H108	S111	R117
GR	R37	R38	E41	E50	K53	K66	K67	W70	R103	Y106	R109	Q115
TGR	R217	D218	N219	Q220	E259	R260	R393	R414	D433	R450	Y451	R454
TR	R121	E122	K123	K124	E163	R164	R293	K315	D334	R351	L352	Q355
GR	T119	K120	S121	H122	G158	M159	R291	H312	D331	R347	K348	H351
TGR	E478	H502	K506	E509	W510	H514	R515	E516	D517	V519	G545	E546
TR	E379	H403	W407	E410	W411	S415	R416	D417	N418	K420	G446	E447
GR	P376	S400	T404	Y407	H408	T411	K414	-	-	K416	D441	E442
TGR	K561	D565	R566	H571	E576	T577	H582					
TR	K462	D466	S467	H472	E477	V478	S483					
GR	K457	D461	N462	H467	E472	E473	R478					

Fig. 10. Alignment of the charged residues (positively charged residues – histidine, lysine, arginine and negatively charged residues – aspartic acid, glutamic acid) within a sphere of radius 15 Å around GSSG. Negatively charged residues are shown in red and positively charged in green. These residues account for +12 unit charge around the ligand in GR, +9 in TGR and +7 in GR.

Table 5
Docking scores in kcal/mol obtained by docking GSSG in GR (1GRA), TR (2J3N), SmTGR crystal structure (2V6O) and SmTGR homology model.

S. no.	Protein	PDB	Docking scores
1	GR	1GRA	−244.35
2	TR	2J3N	−81.36
3	SmTGR	2V6O	−145.86
4	SmTGR	Homology Model	−138.97

Table 6
Binding scores in kcal/mol obtained from docking of inhibitors extracted from GR-ligand complexes, the PDB codes for GR-inhibitor complexes, and ligands used for docking.

S. no.	PDB	Ligand	Score
1	1XAN	Xanthene-der[a]	−35.93
2	1BWC	Adjoene-der	−15.36
3	2GH5	Menadione-der	−28.04

[a] der: derivative.

protein GR for which the GR-inhibitor complexes are known. Also the conformational space of these ligands was explored in the active site disulfide region near the FAD site and in the dimer interface region. Three crystal structures of GR-inhibitor complexes, 1XAN [37], 1BWC [38] and 2GH5 [39] were analyzed and compared with the corresponding ligand binding pockets in SmTGR model. Though the ligands in 1BWC and 2GH5 are covalently bound to the active site disulfide Cys58, non-covalent docking in the SmTGR model has been carried out. Different options were tried to obtain the best binding conformations close to the binding mode of these ligands in GR, e.g. defining rotatable bonds and hydrogen bonding sites improved the docking scores. Each run generated 20 different binding poses for each of the ligands. Table 6 shows the binding scores of the best docked conformations of the ligands. A variety of conformations were obtained during the docking process which indicated that the pockets enclosing the ligands are quite spacious and could be explored for designing better ligands.

The xanthene derivative (1XAN) [37], which is a non-competitive inhibitor, binds at the interface region of GR dimer. It is a symmetrical molecule that makes important interactions with residues from both the chains (Fig. 11). *Pi*-stacking interactions with Phe78 from both monomers sandwich the xanthene tricyclic ring. His75 and His82 are at H-bonding distance from the propionic acid side chain of the ligand. Other residues lining the inhibitor pocket around the xanthene ring are Asn71, Val74 and Tyr407. Three water molecules close to the ligand form H-bonds with the xanthene ring. In SmTGR, the framework of residues surrounding the ligand is different. *Pi*-stacking interactions corresponding to Phe78 are not observed. These are substituted by other hydrophobic interactions with Leu170 from both the monomers. His75 and His82 in GR are substituted by non-polar residues, such as Leu171 and Ala178, respectively, which form hydrophobic interactions with the ligand. H-bonds are observed between the xanthene ring and the side chains of Gln167 and Glu509. These residues in GR correspond to Asn71 and Tyr407 (Fig. 11).

The adjoene derivative in GR (1BWC) [38] is found in the same pocket where GSSG binds and is covalently linked to disulfide active site residue Cys58. Backbones of Ser30 and Ala34 show H-bonds with the sulfoxide oxygen of the ligand. Other residues, which are found proximal to the ligand, include Leu33, Val59, Arg37, Arg347, Ile343, Thr339 and Tyr114. Adjoene derivative in TGR, although placed in the same pocket, lies farther at a distance of 5 Å from the active site Cys154 in comparison to GR, as the

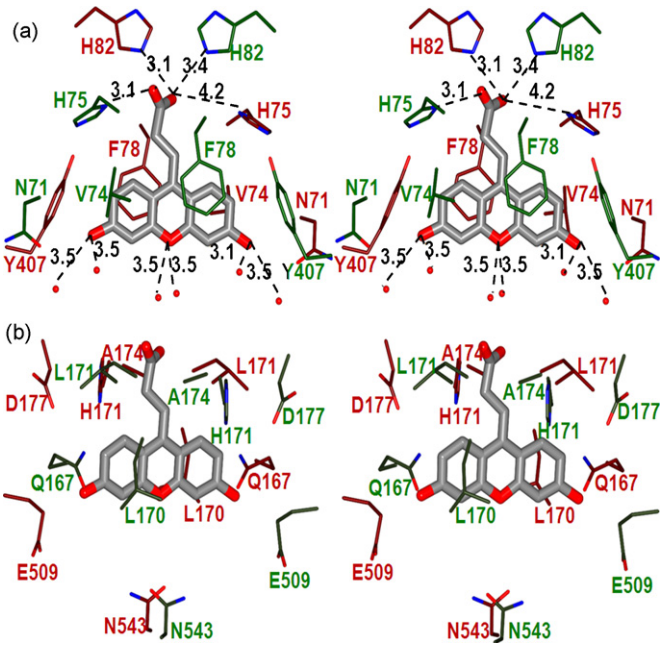

Fig. 11. (a) Interactions of the inhibitor xanthene derivative (3,6-dihydroxy-xanthene-9-propionic acid in licorice) in GR crystal structure 1XAN. It forms important *pi*-stacking interaction with Phe78. (b) However, in TGR, corresponding *pi*-stacking interactions are substituted by hydrophobic interactions with Leu150. Residues corresponding to monomer 1 are shown in maroon and those corresponding to monomer 2 are in dark green.

covalent link is missing between the ligand and this Cys residue. Ser117 and Ala121 are found in SmTGR in place of Ser30 and Ala34 in GR. All the other interacting residues are conserved such as Leu120, Val155, Arg450, Ile446, Thr442 and Tyr212 except Arg37 which is replaced by Lys124. Some of these residues exhibit interactions with GSSG as mentioned before (Table 4).

The fluoro derivative of menadione in 2GH5 [39] is also found in the GSSG binding site, covalently bonded to Cys58. The keto group of naphthoquinone moiety is H-bonded to His467 of the second monomer. The carboxylate group of ligand side chain shows H-bonds with Tyr114, Arg37 and Arg347 as is seen in case of the substrate GSSG. Other important residues surrounding the ligand are Ser30, Leu33, Ala34, Val64, Leu110, and Thr339. In SmTGR, ligand binding pocket shows similar conserved residues. The naphthoquinone ring is H-bonded to a His571 as in GR. The residues around the ligand corresponding to GR are Ser117, Leu120 and Leu208. However certain close contacts with Tyr212 (Tyr114 in GR) and Ala121 (Ala34 in GR), are observed that need to reorient for accommodating the ligand.

Thus from the above analysis, we find that the residues in active site disulfide region near the FAD site are conserved in GR and SmTGR. No major differences are observed in the binding pattern of ligands in both the cases. However, the dimer interface region shows distinct variations in SmTGR as compared to GR.

4. Conclusions

A homology model of SmTGR has been generated in the fully functional dimeric form with cofactors FAD and NADP(H) in two different conformations: reducing and non-reducing. The minimized and refined model, as assessed qualitatively by PROCHECK was compared with the recently solved crystal structure of SmTGR in the monomeric form with FAD, but lacking NADP(H) and the SeC motif. The homology model was found to be quite similar in the TR region although the Grx part seemed to be in a slightly different

orientation. This can be attributed to the flexible linker loop connecting Grx and TR domains. Hinge movements, studied by steered molecular dynamics of Grx domain demonstrated the movement of Grx domain towards the TR domain to adopt the 'closed' form, where the SeC tail of the second monomer can easily shuttle electrons from the redox active site to the first monomer. In order to understand the GR functions of SmTGR, the GSSG (substrate) binding pocket was studied in comparison to GR and TR. Docking studies of GSSG and electrostatic potential calculations of GSSG binding pocket indicate that TGR is favorable for GSSG binding in contrast to TR. This explains why SmTGR can reduce GSSG whereas TR cannot. Docking of inhibitors from GR-inhibitor complexes in the disulfide active site and the dimer interface region was also analyzed in SmTGR model and compared to parent GR complexes, which showed plausible analogous binding pockets in SmTGR.

Acknowledgements

MS acknowledges CSIR for senior research fellowship. AM and SK acknowledge Department of Biotechnology, Govt. of India, for providing partial support to this work vide Grant No. BT/PR5767/PID/06/260/2005.

Appendix A. Supplementary data

Supplementary data associated with this article can be found, in the online version, at doi:10.1016/j.jmgm.2008.10.009.

References

[1] L. Chitsulo, P. Loverde, D. Engels, Schistosomiasis, Nat. Rev. Microbiol. 2 (2004) 12–13.
[2] M. Lebens, J.-B. Sun, C. Czerkinsky, J. Holmgren, Current status and future prospects for a vaccine against schistosomiasis, Exp. Rev. Vacc. 3 (3) (2004) 315–328.
[3] S.A. Williams, D.A. Johnston, Helminth genome analysis: the current status of the filarial and schistosome genome projects. Filarial Genome Project. Schistosome Genome Project, Parasitology 118 (1999) S19–S38.
[4] G. Salinas, M.E. Selkirk, C. Chalar, R.M. Maizels, C. Feranadez, Linked thioredoxin-glutathione systems in platyhelminths, Trends Parasitol. 20 (7) (2004) 340–346.
[5] A. Holmgren, C. Johansson, C. Berndt, M.E. Lonn, C. Hudemann, C.H. Lillig, Thiol redox control via thioredoxin and glutaredoxin systems, Biochem. Soc. Trans. 33 (6) (2005) 1375–1377.
[6] P.A. Karplus, G.E. Schulz, The refined structure of glutathione reductase at 1.54 Å resolution, J. Mol. Biol. 195 (1987) 701–729.
[7] P.R.E. Mittl, G.E. Schulz, Structure of glutathione reductase from *Escherichia coli* at 1.86 Å resolution: comparison with the enzyme from human erythrocytes, Prot. Sci. 3 (1994) 799–809.
[8] V.N. Gladyshev, K.T. Jeang, T.C. Stadtman, Selenocysteine, identified as the penultimate C-terminal residue in human T-cell thioredoxin reductase, corresponds to TGA in the human placental gene, Proc. Natl. Acad. Sci. U.S.A. 93 (1996) 6146–6151.
[9] Q.-A. Sun, Y. Wu, F. Zappacosta, K.-T Jeang, B.J. Lee, D.L. Hatfield, V.N. Gladyshev, Redox regulation of cell signaling by selenocysteine in mammalian thioredoxin reductases, J. Biol. Chem. 274 (35) (1999) 24522–24530.
[10] J. Jurado, M.-J. Prieto-Álamo, J. Madrid-Rísquez, C. Pueyo, Absolute gene expression patterns of thioredoxin and glutaredoxin redox systems in mouse, J. Biol. Chem. 278 (2003) 45546–45554.
[11] Q.-A. Sun, D. Su, S.V. Novoselov, B.A. Carlson, D.L. Hatfield, V.N. Gladyshev, Reaction mechanism and regulation of mammalian thioredoxin/glutathione reductase, Biochemistry 44 (2005) 14528–14537.
[12] Q.-A. Sun, L. Kirnarsky, S. Sherman, V.N. Gladyshev, Selenoprotein oxidoreductase with specificity for thioredoxin and glutathione systems, Proc. Natl. Acad. Sci. U.S.A. 98 (7) (2001) 3673–3678.
[13] D. Su, S.V. Novoselov, Q.-A. Sun, M.E. Moustafa, Y. Zhou, R. Oko, D.L. Hatfield, V.N. Gladyshev, Mammalian selenoprotein thioredoxin-glutathione reductase, J. Biol. Chem. 280 (2005) 26491–26498.
[14] L. Zhong, S.J.E. Arner, A. Holmgren, Structure and mechanism of mammalian thioredoxin reductase: the active site is a redox-active selenolthiolyselenenyl-sulfide formed from the conserved cysteine-selenocysteine sequence, Proc. Natl. Acad. Sci. U.S.A. 97 (1) (2000) 5854–5859.
[15] H.M. Alger, D.L. Williams, The disulfide redox system of *Schistosoma mansoni* and the importance of a multifunctional enzyme, thioredoxin glutathione reductase, Mol. Biochem. Parasitol. 121 (2002) 129–139.
[16] A.N. Kuntz, E. Davioud-Charvet, A.A. Sayed, L.L. Califf, J. Dessolin, E.S.J. Arner, D.L. Williams, Thioredoxin glutathione reductase from *Schistosoma mansoni*: an essential parasite enzyme and a key drug target, PLoS Med. 4 (6) (2007) 1071–1086.
[17] F. Angelucci, A.E. Miele, G. Boumis, D. Dimastrogiovanni, M. Brunori, A. Bellelli, Glutathione reductase and thioredoxin reductase at the crossroad: the structure of *Schistosoma mansoni* thioredoxin glutathione reductase, 72(3) (2008) 936–945.
[18] G. Waksman, T.S.R. Krishna, C.H. Williams Jr., J. Kuriyan, Crystal structure of *Escherichia coli* thioredoxin reductase refined at 2 Å resolution. Implications for a large conformational change during catalysis, J. Mol. Biol. 236 (1994) 800–816.
[19] E.I. Biterova, A.A. Turanov, V.N. Gladyshev, J.J. Barycki, Crystal structures of oxidized and reduced mitochondrial thioredoxin reductase provide molecular details of the reaction mechanism, Proc. Natl. Acad. Sci. U.S.A. 102 (2005) 15018–15023.
[20] K. Fritz-Wolf, S. Urig, K. Becker, The structure of human thioredoxin reductase 1 provides insights into C-terminal rearrangements during catalysis, J. Mol. Biol. 370 (2007) 116–127.
[21] Y. Feng, N. Zhong, N. Rouhier, T. Hase, M. Kusunoki, J.P. Jacquot, C. Jin, B. Xia, Structural insight into poplar glutaredoxin C1 with a bridging iron-sulfur cluster at the active site, Biochemistry 45 (2006) 7998–8008.
[22] Y. Yang, S. Jao, S. Nanduri, D.W. Starke, J.J. Mieyal, J. Qin, Reactivity of the human thioltransferase (glutaredoxin) C7S, C25S, C78S, C82S mutant and NMR solution structure of its glutathionyl mixed disulfide intermediate reflect catalytic specificity, Biochemistry 37 (1998) 17145–17156.
[23] S.K. Katti, A.H. Robbins, Y. Yang, W.W. Wells, Crystal structure of thioltransferase at 2.2 Å resolution, Prot. Sci. 4 (1995) 1998–2005.
[24] J.E. Debreczeni, C. Johansson, K. Kavanagh, P. Savitsky, M. Sundstrom, C. Arrowsmith, J. Weigelt, A. Edwards, F. Von Delft, U. Oppermann, Crystal structure of human thioredoxin reductase 1, http://dx.doi.org/10.2210/pdb2cfy/pdb.
[25] T. Sandalova, L. Zhong, Y. Lindqvist, A. Holmgren, G. Schneider, Three-dimensional structure of a mammalian thioredoxin reductase: implications for mechanism and evolution of a selenocysteine-dependent enzyme, Proc. Natl. Acad. Sci. U.S.A. 98 (2001) 9533–9538.
[26] B.E. Eckenroth, M.A. Rould, R.J. Hondal, S.J. Everse, Structural and biochemical studies reveal differences in the catalytic mechanisms of mammalian and *Drosophila melanogaster* thioredoxin reductases, Biochemistry 46 (2007) 4694–4705.
[27] A. Fiser, A. Sali, Modeller: generation and refinement of homology-based protein sequence models, Methods Enzymol. 374 (2003) 461–491.
[28] SYBYL 7.1, Tripos International, 1699 South Hanley Rd., St. Louis, Missouri, 63144, USA.
[29] Two additional models were prepared from templates with cofactors in the same conformation. For modeling SmTGR with cofactors in conformation I, all templates with cofactors in reducing *pi*-stacked orientation were taken: 1ZDL (sequence identity 54%), 1GRB (36%), 1GET (36%) and 1GEU (36%). The latter three are GRs, since only one TR structure is available with cofactors in this conformation. For modeling SmTGR with cofactors in conformation II, templates with cofactors in non-*pi*-stacked orientation were taken: 1H6V (60%) 2NVK (51%) and 2J3N (61%). These models have been referred to as Model 2 and Model 3 respectively. Grx domain was modeled as in Model 1. Fig. S3 shows the superposition of these models with Model 1. There are no significant structural differences in the TR domain of all the models, including the binding pockets of the cofactors in two different conformations. Therefore, SmTGR Model 1 has been used for all analysis.
[30] J.C. Phillips, R. Braun, W. Wang, J. Gumbart, E. Tajkhorshid, E. Villa, C. Chipot, R.D. Skeel, L. Kale, K. Schulten, Scalable molecular dynamics with NAMD, J. Comp. Chem. 26 (2005) 1781–1802.
[31] W.L. Jorgensen, J. Chandrasekhar, J.D. Madura, R.W. Impey, M.L. Klein, Comparison of simple potential functions for simulating liquid water, J. Chem. Phys. 79 (1983) 926–935.
[32] T. Darden, D. York, L. Pedersen, Particle mesh Ewald: An N log (N) method for Ewald sums in large systems, J. Chem. Phys. 98 (1993) 10089–10092.
[33] W. Humphrey, A. Dalke, K. Schulten, VMD-visual molecular dynamics, J. Mol. Graph. 14 (1996) 33–38.
[34] R.A. Laskowski, M.W. MacArthur, D.S. Moss, J.M. Thorton, PROCHECK: a program to check the stereochemical quality of protein structures, J. Appl. Cryst. 26 (1993) 283–291.
[35] P.A. Karplus, G.E. Schulz, Substrate binding and catalysis by glutathione reductase as derived from refined enzyme: substrate crystal structures at 2 Å resolution, J. Mol. Biol. 210 (1989) 163–180.
[36] R. Judson, Genetic algorithms and their use in chemistry, in: K.B. Lipkowitz, D.B. Boyd (Eds.), Reviews in Computational Chemistry, vol. 10, VCH Publishers, New York, 1997, pp. 1–73.
[37] S.N. Savvides, P.A. Karplus, Kinetics and crystallographic analysis of human glutathione reductase in complex with a xanthene inhibitor, J. Biol. Chem. 271 (1996) 8101–8107.
[38] H. Gallwitz, S. Bonse, A. Martinez-Cruz, I. Schlichting, K. Schumacher, R.L. Krauth-Siegel, Ajoene is an inhibitor and subversive substrate of human glutathione reductase and *Trypanosoma cruzi* trypanothione reductase: crystallographic, kinetic, and spectroscopic studies, J. Med. Chem. 42 (1999) 364–372.
[39] H. Bauer, K. Fritz-Wolf, A. Winzer, S. Little, V. Yardley, H. Vezin, B. Palfey, R.H. Schirmer, E. Davioud-Charvet, A fluoro analogue of the menadione derivative 6-[2′-(3′-methyl)-1′,4′-naphthoquinolyl]hexanoic acid is a suicide substrate of glutathione reductase. Crystal structure of the alkylated human enzyme, J. Am. Chem. Soc. 128 (2006) 10784–10794.

[40] D. van der Spoel, E. Lindahl, B. Hess, A.R. Buuren, E. Apol, P.J. Meulenhoff, D.P. Tieleman, A.L.T.M. Sijbers, K.A. Feenstra, R. van Drunen, H.J.C. Berendsen, Gromacs User Manual version 3.3, 2005.
[41] W. Schuettelkopf, D.M.F. van Aalten, PRODRG—a tool for high-throughput crystallography of protein–ligand complexes, Acta Cryst. D 60 (2004) 1355–1363.
[42] E. Mitchell, P.J. Artymiuk, D.W. Rice, P. Willett, Use of graph theory to compare secondary structure motifs in proteins, J. Mol. Biol. 212 (1989) 151–166.
[43] L. Potterton, S. McNicholas, E. Krissinel, J. Gruber, K. Cowtan, P. Emsley, G.N. Murshudov, S. Cohen, A. Perrakis, M. Noble, Developments in the CCP4 molecular-graphics project, Acta Cryst. D 60 (2004) 2288–2294.
[44] S. Urig, J. Lieske, K. Fritz-Wolf, A. Irmler, K. Becker, Truncated mutants of human thioredoxin reductase 1 do not exhibit glutathione reductase activity, FEBS Lett. 580 (15) (2006) 3595–3600.
[45] J.L. Rendon, I.P. del Arenal, A. Guevara-Flores, A. Uribe, A. Plancarte, G. Mendoza-Hernandez, Purification, characterization and kinetic properties of the multi-functional thioredoxin-glutathione reductase from *Taenia crassiceps* metacestode (cysticerci), Mol. Biochem. Parasitol. 133 (1) (2004) 61–69.
[46] S.M. Kanzok, A. Fechner, H. Bauer, J.K. Ulschmid, H.M. Müller, J. Botella-Munoz, S. Schneuwly, R. Schirmer, K. Becker, Substitution of the thioredoxin system for glutathione reductase in *Drosophila melanogaster*, Science 291 (5504) (2001) 643–646.